

Neutrino-Nucleus Cross Section: Fermi Gas Model vs. Spectral function

Hiroki Nakamura^a and Ryoichi Seki^{b,c}

^aDepartment of Physics, Waseda University, Tokyo 169-8555, Japan

^bW.K. Kellogg Radiation Laboratory,
California Institute of Technology, Pasadena, California 91125

^cDepartment of Physics and Astronomy,
California State University, Northridge, California 91330

Quasi-elastic cross sections of $^{16}\text{O}(\nu_\mu, \mu^-)$ are calculated using a realistic spectral function at various scattering angles and are compared with those of the Fermi gas model. Similar comparison is also made for cross sections of quasi-free Δ resonance production.

1. Introduction

Quasi-elastic neutrino-nucleus cross section is not a simple sum of the elastic neutrino-nucleon cross sections because of significant nuclear effects. The effects include final-state interactions, binding effects of the nucleons in the initial nucleus, and corrections caused by many-body interactions. In the NuInt01 Workshop, we reported the first part of our calculations of quasi-elastic cross sections of the neutrino-oxygen charged-current reactions [1]. In the report, we described our formalism and showed calculations using Fermi gas model and a nuclear spectral function. In the present report, we make detailed comparison of the quasi-elastic cross sections using the two methods and also do the same for quasi-free Δ resonance production.

After presenting a brief account of our formalism in Section 2, we describe the models used in our calculation in Section 3. Our numerical results are shown in Section 4 for the quasi-elastic scattering and in Section 5 for the quasi-free Δ resonance production. We present our conclusion in Section 6.

2. Neutrino-Nucleus Differential Cross Section

In this section, we present a brief account of our formalism used for our calculations. More detailed account of the formalism is found in our first report [1].

The quasi-elastic neutrino-nucleus cross section of $^{16}\text{O}(\nu_\mu, \mu)$ is expressed as

$$\frac{d\sigma}{d\omega d\cos\theta} = \frac{k_\ell}{4(2\pi)^3 M_T^2 E_\nu} \int d^3\mathbf{p} F(\mathbf{p}, \mathbf{q}, \omega) |\mathcal{M}_{\nu N}|^2. \quad (1)$$

Here, E_ν is the incident neutrino energy, k_ℓ the scattered muon momentum, M_T the target nuclear mass, and ω and \mathbf{q} the energy and momentum transfer to the nucleus, respectively. $\mathcal{M}_{\nu N}$ is the invariant amplitude of the neutrino-nucleon charged-current reaction $n(\nu, \mu)p$, which can be expressed as a function of Mandelstam variables s , t and u . $F(\mathbf{p}, \mathbf{q}, \omega)$ accounts for physics of the nuclear initial state and also for effects from final state interactions. It is expressed as the imaginary part of the single-particle and single-hole propagator. Adopting the factorization approximation that the propagator is expressed as a convolution of single-particle propagator and single-

hole propagator, we write

$$F(\mathbf{p}, \mathbf{q}, \omega) = \frac{M_T}{(2\pi)^2 V} \times \int \frac{d\omega'}{p^0(p^0 + \omega)} P_h(\mathbf{p}, \omega') P_p(\mathbf{p} + \mathbf{q}, \omega - \omega'), \quad (2)$$

where V is the spatial volume for normalization. The single-hole propagator $P_h(\mathbf{p}, \omega)$ includes all information about the initial nuclear state, and the single-particle propagator $P_p(\mathbf{p}, \omega)$ includes the nuclear final-state interactions. $P_h(\mathbf{p}, \omega)$ and $P_p(\mathbf{p}, \omega)$ are expressed as the imaginary parts of single-hole propagator and single-particle propagator, respectively, and are given by

$$P_h(\mathbf{p}, \omega) = \langle A | a_{\mathbf{p}}^\dagger \delta(\hat{H} - E_A - \omega) a_{\mathbf{p}} | A \rangle \quad (3)$$

$$P_p(\mathbf{p}, \omega) = \langle A | a_{\mathbf{p}} \delta(\hat{H} - E_A - \omega) a_{\mathbf{p}}^\dagger | A \rangle. \quad (4)$$

Here, $|A\rangle$ is the target nucleus in the ground state with the energy E_A for the Hamiltonian \hat{H} . $a_{\mathbf{p}}^\dagger$ and $a_{\mathbf{p}}$ are the creation and annihilation operators of a nucleon in the nuclear medium, respectively. As it is constructed, $P_h(\mathbf{p}, \omega)$ is interpreted as the probability of finding a nucleon in the nucleus, with the momentum \mathbf{p} and the removal energy ω , and is referred to a spectral function. $P_p(\mathbf{p}, \omega)$ gives the energy-momentum spectrum of the knocked-out nucleon.

For the calculation of the quasi-elastic cross sections, $P_h(\mathbf{p}, \omega)$ and $P_p(\mathbf{p}, \omega)$ thus contain the vital nuclear effects, and are quite important to be included appropriately. In this work, we focus on $P_h(\mathbf{p}, \omega)$.

3. Various Models

We examine three versions of Fermi gas model and the spectral function. While the first three are simple models and some of them have been used in practice, we consider the fourth to be most realistic and to be used in serious calculations.

a. Fermi Gas

The target nucleus is taken to be a relativistic Fermi gas of the nucleons at zero temperature. In this model, P_h and P_p are expressed as

$$P_h(\mathbf{p}, \omega) = \delta(E_{\mathbf{p}} - E_B + \omega) V \theta(p_F - |\mathbf{p}|)$$

$$P_p(\mathbf{p}, \omega) = \delta(E_{\mathbf{p}} - \omega) V \theta(|\mathbf{p}| - p_F), \quad (5)$$

where $E_{\mathbf{p}} = \sqrt{\mathbf{p}^2 + M^2}$ and p_F is the Fermi momentum. E_B is the binding energy of the nucleon in the initial ground-state nucleus, effectively represented by a single constant energy. V is written as $V = 3\pi^2 N/p_F^3$ in terms of the number of the neutrons in the nucleus, N . In the final state, the knock-out nucleon is assumed to suffer no nuclear binding effect by setting $E_B = 0$. We use $p_F = 225$ MeV and $E_B = 25$ MeV for the oxygen nucleus, taken from an electron scattering analysis [3].

b. Fermi Gas without Pauli Blocking (FG w/o PB)

As Eq. (5) shows, the knocked-out nucleon momentum is restricted to be greater than the Fermi momentum because of the Pauli exclusion principle. The restriction is usually referred as the Pauli blocking. In this model, we artificially remove the restriction, thereby neglecting the final-state interaction in the Fermi gas model. We thus set

$$P_h(\mathbf{p}, \omega) = \delta(E_{\mathbf{p}} - E_B + \omega) V \theta(p_F - |\mathbf{p}|) \\ P_p(\mathbf{p}, \omega) = V \delta(E_{\mathbf{p}} - \omega). \quad (6)$$

The Pauli blocking is a simple form of the final-state interaction. The difference between the preceding (a.) Fermi gas model and this model gives the degree of the final-state interaction effect in this simple description of the scattering. For the purposes of comparison, we use the same $p_F = 225$ MeV and $E_B = 25$ MeV as above.

c. Fermi gas with Nuclear Potential (Potential)

In the preceding Fermi gas models, (a.) Fermi gas and (b.) FG w/o PB, the binding energy of the nucleon is represented by a constant as an effective parameter. Nuclear binding is a complicated effect resulted from many-body interactions. As a step towards making the calculation more realistic, we incorporate the momentum dependence of the binding effect by introducing the momentum-dependent nuclear potential [4] in the energy balance of the initial state. We write

$$P_h(\mathbf{p}, \omega) = \delta(E_{\mathbf{p}} + V(|\mathbf{p}|) + \omega) V \theta(p_F - |\mathbf{p}|)$$

(7)

$$P_p(\mathbf{p}, \omega) = \delta(E_p + V(|\mathbf{p}|) - \omega) \times V\theta(|\mathbf{p}| - p_F)\theta(E_p + V(|\mathbf{p}|) - M), \quad (8)$$

where M is the nucleon mass and $V(|\mathbf{p}|)$ is the nuclear potential. Note that the difference between (a.) Fermi gas and this model is a replacement of $-E_B$ by $V(|\mathbf{p}|)$ in (a.) and the inclusion of $V(|\mathbf{p}|)$ in P_p of (a.) The step function for P_p in Eq. (8) guarantees the nucleon gets knocked out with a positive energy. We use $V(|\mathbf{p}|)$ of Ref. [4], together with $p_F = 217$ MeV as specified there.

d. Spectral Function

In the preceding models, $P_h(\mathbf{p}, \omega)$, the spectral function, is expressed as the delta functions. In the real nucleus, the nucleons have a distribution of momentum and (removal) energy. we adopt a realistic spectral function, obtained by a many-body calculation. The spectral function was calculated by Benhar et al.[5] for ^{12}C and was modified by us, suitable for ^{16}O as described in our first report [1]. The ^{12}C spectral function was constructed with single-particle distribution in combination with local density approximation on an elaborate correlated-basis many-body calculation of nuclear matter, and has been applied to electron-nucleus scattering, as described in Ref. [5]. In order to clarify the effect of the spectral function, we neglect the final-state interaction and set

$$P_p(\mathbf{p}, \omega) = V\delta(E_p - \omega). \quad (9)$$

4. Numerical Results

In Figs. 1–8, we illustrate the differential cross sections of the quasi-elastic $^{16}\text{O}(\nu_\mu, \mu^-)$ scattering, calculated using the models described above.

In Figs. 1–8, we see the curves for the spectral function model have long tails for large energy transfers, while no such tails are seen for the other models. The tails represent the contribution from short-range nucleon correlations in the nucleus, which other models do not include.

Figures 1–4 show that the spectral function model gives a substantially smaller but wider contribution than the other models at small angles, while the difference is much reduced at large an-

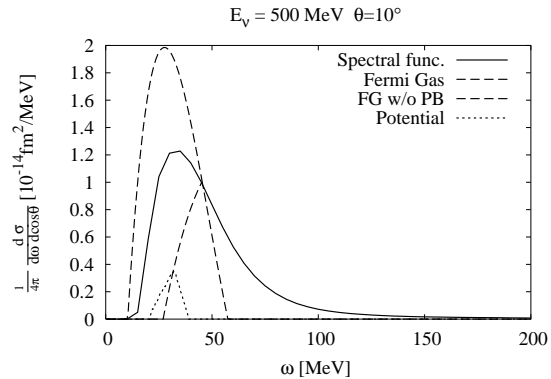


Figure 1. Differential cross section of quasi-elastic $^{16}\text{O}(\nu_\mu, \mu)$ scattering as a function of the energy transfer ω for the muon scattering angle $\theta = 10^\circ$. The incident energy of neutrino is 500 MeV. The solid curve is the result for (d.) the spectral function model, the upper dashed curve for (b.) the Fermi gas model without Pauli blocking (FG w/o PB), the lower dashed curve for (a.) the Fermi gas model, and the dotted curve for (c.) the Fermi gas model with nuclear potential (potential).

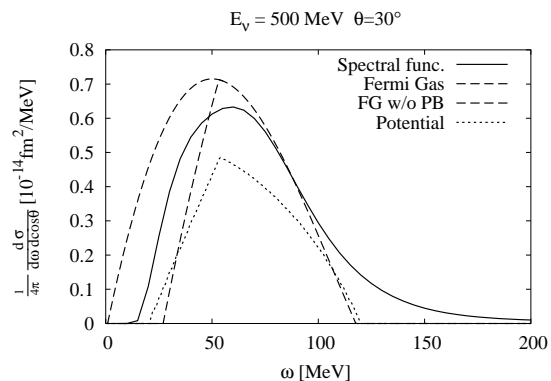


Figure 2. Same as Fig. 1, but for $\theta = 30^\circ$.

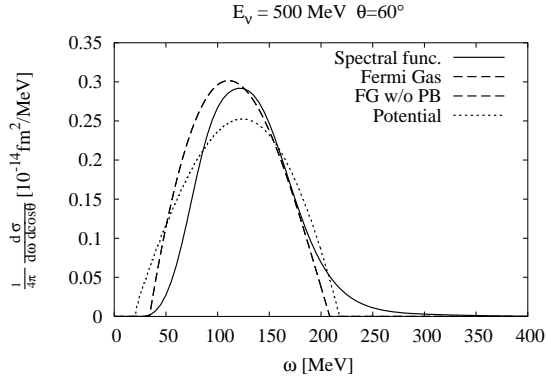


Figure 3. Same as Fig. 1, but for $\theta = 60^\circ$.

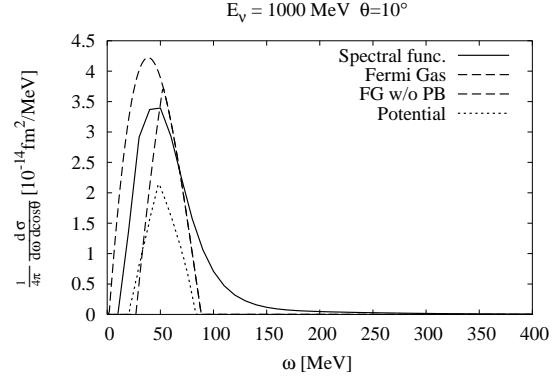


Figure 5. Same as Fig. 1, but the incident neutrino energy is 1000 MeV and for $\theta = 10^\circ$.

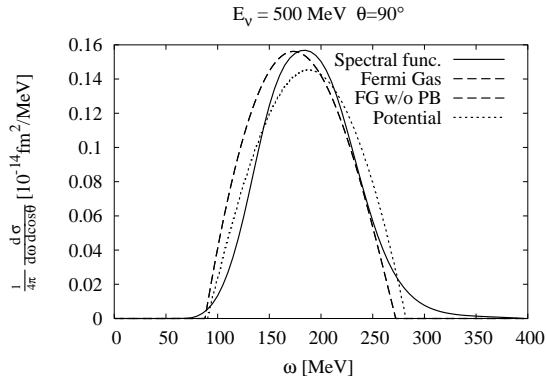


Figure 4. Same as Fig. 1, but for $\theta = 90^\circ$.

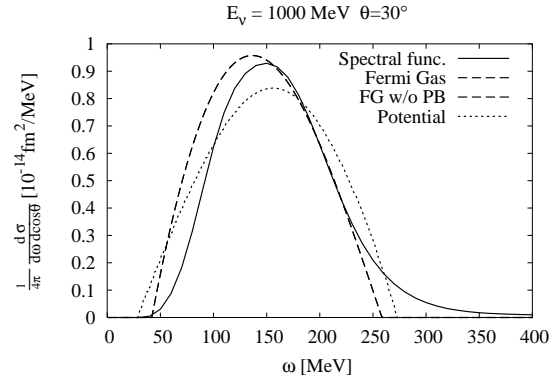


Figure 6. Same as Fig. 1, but the incident neutrino energy is 1000 MeV and for $\theta = 30^\circ$.

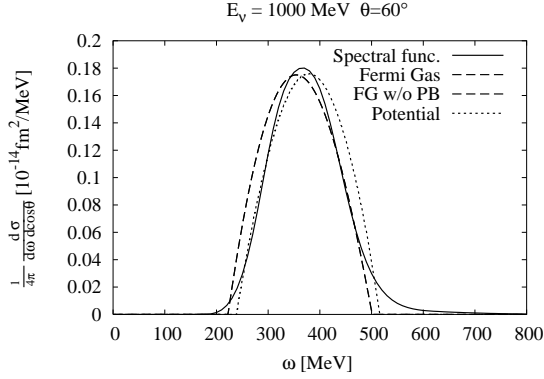


Figure 7. Same as Fig. 1, but the incident neutrino energy is 1000 MeV and for $\theta = 60^\circ$.

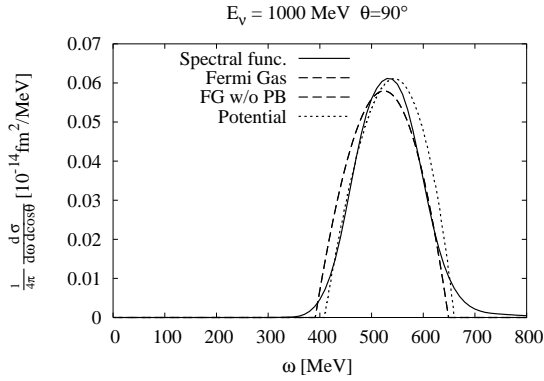


Figure 8. Same as Fig. 1, but the incident neutrino energy is 1000 MeV and for $\theta = 90^\circ$.

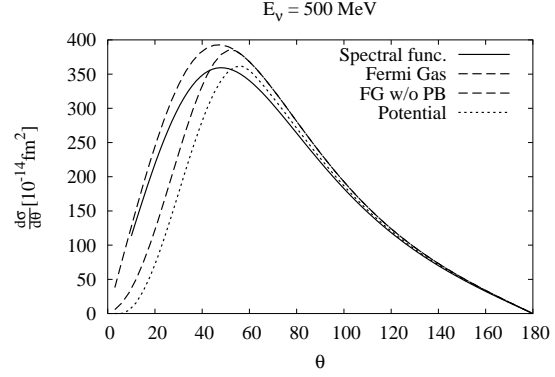


Figure 9. Differential cross section of quasi-elastic $^{16}\text{O}(\nu_\mu, \mu)$ scattering as a function of muon scattering angle θ . The incident energy is 500 MeV. The curves correspond to the results of different models in the same way as in Fig. 1.

gles. Comparing Figs. 1–4 and Figs. 5–8, we find that this feature becomes much less prominent as the incident neutrino energy increases from 500 MeV to 1000 MeV.

Because of the tail contributions noted above, the differential cross section integrated over the energy transfer is close to each other among the four models, as seen in Figs. 9 and 10. There are some variation remain for small scattering angle.

Figures 1–8 also show that the cross section of the Fermi gas is smaller than that of the Fermi gas without Pauli blocking. Furthermore, the cross section of the Fermi gas with nuclear potential is smaller than that of the Fermi gas. These differences are caused by whether and how the final-state interactions are included. The inclusion of the final-state interaction reduces the cross section.

In this work, we do not include effects of the final-state interaction in the spectral function model. The preceding consideration suggests, however, that the cross section by the spectral function model would be reduced upon inclusion of the final-state interaction.

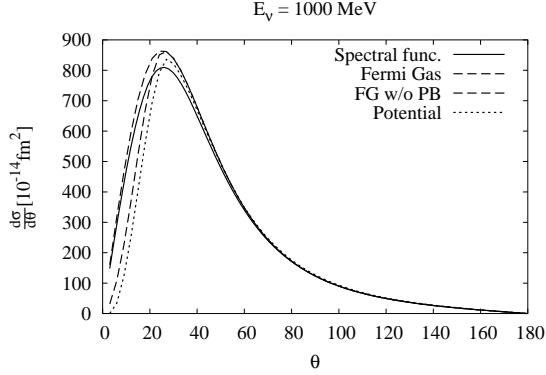


Figure 10. Same as Fig. 9, but the incident energy is 1000 MeV.

5. Quasi-free Δ Resonance Production

In our first report, we showed differential cross sections of the quasi-free Δ resonance production in the Fermi gas models. Here, we compare the cross sections with the one using the spectral function.

The cross sections of the quasi-free Δ resonance production are calculated using a formalism similar to that of the quasi-elastic scattering, as described in the first report [1]. Note that the invariant amplitude and P_p are modified appropriate for the Δ resonance production.

The results are shown in Figs. 11 and 12. We see that the cross section using the spectral function is smaller than that of the Fermi gas model with a tail distribution, as in the case of the quasi-elastic scattering described above and also shown in the same figures for comparison.

6. Conclusion

In both cases of quasi-elastic scattering and quasi-free Δ resonance production, the spectral function yields smaller differential cross sections as a function of the energy transfer with tails for large energy transfer, in comparison to different version of the Fermi gas model. The difference is reduced in the differential cross sections after the energy transfer is integrated, except some varia-

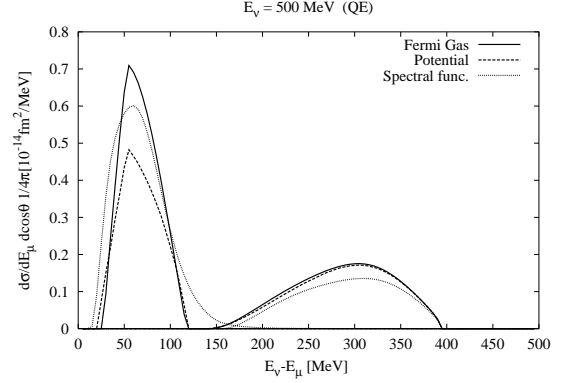


Figure 11. Differential cross section of quasi-free $^{16}\text{O}(\nu_\mu, \mu)$ Δ resonance production (left curves) and of quasi-elastic $^{16}\text{O}(\nu_\mu, \mu)$ scattering (right curves) as a function of the energy transfer. The incident energy is 500 MeV, and the scattering angle is 30° . The dotted curve is for (d.) the spectral function model, the dashed curve is for (c.) the Fermi gas model with nuclear potential, and the solid curve for (a.) the Fermi gas model.

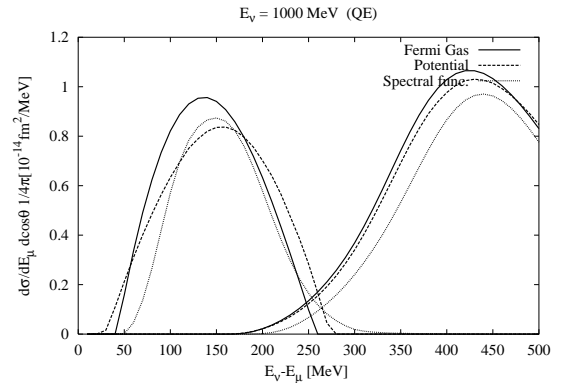


Figure 12. Same as Fig. 11, but the incident energy is 1000 MeV.

tion remains for small scattering angle.

We thank Omar Benhar for making ^{12}C spectral function available to us. This work is supported by the U. S. Department of Energy under grant DE-FG03-87ER40347 at CSUN and the U. S. National Science Foundation under grant 0244899 at Caltech.

REFERENCES

1. H. Nakamura and R. Seki, Nucl. Phys. Proc. Suppl. **112** (2002) 197. See also references therein.
2. R. A. Smith and E. J. Moniz, Nucl. Phys. **B43** (1972) 605.
3. E.J. Moniz, I. Sick, R.R. Whitney, J.R. Ficenec, R.D. Kephart and W.P. Trower, Phys. Rev. Lett. **26** (1971) 445.
4. For example, F.A. Brieva and A. Dellafiore, Nucl. Phys. A **292** (1977) 445.
5. Private communication from O. Benhar. The method of the calculation is described in: O. Benhar, A. Fabrocini, S. Fantoni, and I. Sick, Nucl. Phys. **A579** (1994) 493; and references therein.